Title: Noncaloric monosaccharides induce excessive sprouting angiogenesis in zebrafish via foxo1a-marcksl1a signal

Running title: Noncaloric Monosaccharides Induce Excessive Angiogenesis

Xiaoning wang[1, *], Jinxiang Zhao[1, 2, *], Jiehuan Xu[3, *], Bowen Li[1], Xia Liu[3, #], Gangcai Xie[3, #], Xuchu Duan[1, #], Dong Liu[1, #]

1 School of Life Science, Nantong Laboratory of Development and Diseases; The Key Laboratory of Neuroregeneration of Jiangsu and Ministry of Education, Co-innovation Center of Neuroregeneration, Nantong University, Nantong, China

2 Suqian First Hospital, Suqian, China

3 Medical School, Nantong University, Nantong, China

[*], These authors contributed equally to this work.

[#], Authors for correspondence:

Dong Liu, Ph.D

School of Life Sciences, Jiangsu Key Laboratory of Neuroregeneration, Nantong University

Building 15-C1213, Seyuan Road 9#, Nantong, China, 226001

Phone: + (86) - 18605133927

Fax: + (86) - 513 - 85511585

Email: liudongtom@gmail.com; tom@ntu.edu.cn

Abstract

Artificially sweetened beverages containing noncaloric monosaccharides were suggested as healthier alternatives to sugar-sweetened beverages. Nevertheless, the potential detrimental effects of these noncaloric monosaccharides on blood vessel function remain inadequately understood. Presently, we have established a zebrafish model that exhibits significant excessive angiogenesis induced by high glucose, resembling the hyperangiogenic characteristics observed in proliferative diabetic retinopathy (PDR). Utilizing this model, we observed that glucose and noncaloric monosaccharides could induce excessive formation of blood vessels, especially intersegmental vessels (ISVs). The excessively branched vessels were observed to be formed by ectopic activation of quiescent endothelial cells (ECs) into tip cells. Single-cell transcriptomic sequencing analysis of the endothelial cells in the embryos exposed to high glucose revealed an augmented ratio of capillary ECs, proliferating ECs, and a series of upregulated proangiogenic genes. Further analysis and experiments validated that foxo1a mediated the excessive angiogenesis induced by monosaccharides by down-regulating the expression of *marcksl1a*. This study has provided new evidence showing the negative effects of noncaloric monosaccharides on the vascular system and the underlying mechanisms.

Key words: noncaloric monosaccharides; endothelial cell activation; foxo1a; marcksl1a; zebrafish

45 **Introduction**

46 Diabetes mellitus (DM) encompasses a group of chronic diseases characterized by elevated
47 blood glucose levels. Among patients with DM, cardiovascular complications, especially the
48 direct and indirect effects of hyperglycemia on the human vascular network, persist as the
49 primary cause of morbidity and mortality [1]. The harmful effects of hyperglycemia are
50 closely associated with both microvascular and macrovascular complications, including
51 retinopathy, nephropathy, neuropathy, atherosclerosis, ischemic heart disease, stroke, and
52 peripheral artery disease [2, 3]. Endothelial dysfunction (ECD) is a systemic pathological
53 state exhibiting disrupted integrity, adhesion, altered proliferation capacity, migration, tube
54 formation, and more [4, 5]. High blood glucose levels over long periods have been
55 demonstrated to be associated with vascular dysfunction both *in vivo* and *in vitro* [6, 7].

56 The epidemiological evidence has indicated the positive correlation between risks of
57 cardiovascular disease and DM with the consumption of sugar-sweetened beverages (SSBs)
58 and 100% fruit juices, thereby emphasizing the concerns for the adverse effects of sugar
59 intake on cardiometabolic risk factors, regardless of whether the sugar is added or naturally
60 occurring [8-12]. Artificially sweetened beverages (ASBs), which incorporate noncaloric
61 sweeteners or low-caloric additives, have been suggested as healthy alternatives to SSBs
62 [13]. ASBs contain sugar alcohols and polyols, such as sorbitol, xylitol, maltitol, mannitol,
63 erythritol, isomalt, and lactitol. The consumption of ASBs worldwide has gradually increased
64 in recent years [13-15]. However, accumulating studies in the last decade suggested that ASB
65 consumption might be associated with an increased risk of cardiovascular events and diabetes

[12, 16-23]. Nevertheless, the underlying mechanisms responsible for these findings remain insufficiently documented.

The zebrafish has been recognized as a valuable animal model for studying metabolic diseases, such as hyperglycemia and diabetic complications, due to its functional conservation in glycol metabolism, pancreas structure, glucose homeostasis, adipose biology, and genetic similarities to mammals [24-26]. The combination of embryonic transparency and transgenic lines, wherein endothelial cells are labeled specifically with fluorescent proteins, facilitates the high-resolution imaging analysis of vascular formation *in vivo*. Immersion of zebrafish in glucose solution has been found to induce diabetic complications, including vascular dysfunction [27-30]. Several recent studies have investigated the effects of high glucose on vascular function in the zebrafish model [30-32]. However, the association between noncaloric monosaccharides and vascular dysfunctions, such as excessive angiogenesis, has not been elucidated. Here, we have successfully established a short-term zebrafish model that exhibits significantly excessive angiogenesis similar to the phenotypes observed in proliferative diabetic retinopathy (PDR) induced by glucose treatment. Using this model, we examined the effects of noncaloric monosaccharides on blood vessel development and investigated the molecular mechanisms. Our results provided new evidence for the negative roles of caloric and noncaloric monosaccharides on vascular development.

Results

Establishment of a short-term model of high-glucose-induced excessive angiogenesis

To establish the short-term zebrafish hyperangiogenenic model induced by high-glucose treatment, we immersed the *Tg(fli1aEP:EGFP-CAAX)*^{ntu666} embryos, a transgenic line wherein the endothelial cells were labeled with membrane-bound GFP (Supplementary Figure 1), in glucose solution within a wide range of concentrations and time windows (Supplementary Figure 2). We subsequently measured the glucose concentration in the embryos and found that the glucose concentration in the embryos treated with high glucose was significantly higher than that in the control group (Supplementary Figure 3). We observed that exposing zebrafish embryos at either 24 hours post fertilization (hpf) or 48 hpf to a 6% D-glucose treatment for a duration exceeding 48 hours led to dramatically increased formation of blood vessels (Figure 1, Movie 1 and 2), especially intersegmental vessels (ISVs) in the indicated area (Figure 1b). The hyperbranched endothelial cells were observed to sprout from existing vessels, including the ISVs, dorsal aorta (DA), and dorsal lateral anastomotic vessel (DLAV) (Figure 1) in embryos treated with high glucose. Additionally, these ectopically branched angiogenic sprouts were not perfused by blood flow. Despite the abnormal vessel formation, no significant developmental defects were observed in these treated embryos when examined under a bright field microscope (Supplementary Figure 4a-c). Moreover, no excessive angiogenic phenotype was observed in the embryos treated with 1%, 2%, 3%, and 4% D-glucose within the corresponding time frame (Supplementary Figure 5). In addition, 6% sucrose treatment at the same condition did not lead to any noticeable abnormal phenotype of vessels (Supplementary Figure 4d-h).

108 **Fructose and noncaloric monosaccharides induce excessive angiogenesis**

109 Fructose is a ketonic monosaccharide that is an energy source for living organisms.
110 Therefore, our study investigated the potential effects of fructose on vascular dysfunction in
111 comparison to glucose. The result demonstrated fructose-induced excessive angiogenesis in
112 zebrafish embryos (Supplementary Figure 6). Wondering whether the effects of glucose and
113 fructose on vascular development were mediated by metabolic events, we then conducted the
114 same tests by using other noncaloric monosaccharides, including L-glucose, D-mannose, D-
115 ribose, and L-arabinose, which could not be digested by animals. Interestingly, we observed
116 that all these noncaloric monosaccharides could induce excessive angiogenesis, among which
117 the L-glucose purchased from two companies resulted in a similar phenotype as efficiently as
118 D-glucose did (Figure 2a-h). However, the disaccharides, including lactose, maltose, and
119 sucrose, which were also tested, did not cause significant excessive angiogenic phenotype
120 (Supplementary Figure 4e, f; Supplementary Figure 7). In addition, we also tested the effects
121 of pyruvic acid but did not observe the excessive angiogenic phenotype in the embryos
122 treated with pyruvic acid solution at 50 nm~50 μm concentration (Supplementary Figure 8).
123 Furthermore, we examined the arterial and venous identity of the hyperbranched vessels via
124 live imaging analysis of the high glucose-treated *Tg(flt1:YFP::kdrl:ras-mCherry)* line, in
125 which the YFP expression in the artery was relatively higher than that in the vein [33]. The
126 result revealed that the hyperbranched ectopic vessels comprised arteries and veins (Figure
127 2i, j).

128 **High glucose promotes quiescent endothelial differentiation into tip cells**

129 Given that a high-glucose shock has been observed to induce excessive angiogenesis in 48
130 hpf embryos, it was hypothesized that the shock might play a crucial role in regulating the
131 differentiation of quiescent endothelial cells (ECs) into active tip cell-like cells and their
132 subsequent behaviors. To investigate whether this was the case, we observed the behaviors of
133 these ECs by confocal time-lapse imaging analysis. As shown in the result, in the control
134 *Tg(fli1aEP:EGFP-CAAX)*^{ntu666} embryos, no significant activation of tip cells in the
135 angiogenic sprouts was observed in the generated ISVs, DA, and DLAV in the embryos aged
136 from 48 hpf to 5 dpf. Moreover, only a few ECs in established ISVs, DA, and DLAV
137 extended filopodia, which quickly retracted (Figure 3a-c, Movie 3). However, many ECs
138 initiated sprouting angiogenesis in the high glucose-treated embryos, extended dynamic
139 filopodia to sense the surroundings, and formed excessive ectopic blood vessels (Figure 3d-e,
140 Movie 4). In a snapshot, we observed that some of the ECs protruded long and intricate
141 sprouts simultaneously (Figure 3f), and nearly all the ECs within an ISV underwent the
142 outgrowth of filopodia in some extreme cases (Figure 3g), suggesting that the high glucose
143 treatment induced the endothelial differentiation into tip cell-like cells. Furthermore, we
144 observed that these outgrowths of the ectopic angiogenic sprouts could establish a connection
145 to the neighboring sprouts and vessels and thereby form complicated vascular structures
146 (Figure 1c, f, i, l, p).

147 **Single-cell transcriptomic sequencing analysis of the endothelial cells isolated from**
148 **glucose-treated embryos**

149 We did a single-cell transcriptomic sequencing analysis to gain more insight into the

150 potential mechanism through which glucose activates the endothelial cells. Due to the limited
151 presence of endothelial cells within the zebrafish embryos, the analysis of these cells poses a
152 challenge. Firstly, we isolated the EGFP-positive cells from control and high glucose-treated
153 embryos. Following the proteolytic dissociation of embryos, the EGFP-positive cells were
154 isolated by fluorescence-activated cell sorting (FACS). Around 300-500 zebrafish embryos
155 were used for the ECs collection for each stage. The isolated ECs were analyzed using a
156 large-scale scRNA-seq (10X Genomics) platform, and the pipeline is illustrated in the
157 diagram (Figure 4a). Multiple criteria were applied to select the single cells, including the
158 retention of the genes that were expressed (Unique Molecular Identifiers or UMI larger than
159 0) in at least 3 individual cells, the selection of cells with the gene expression count falling
160 within the range of 500 to 3000, and the imposition of a threshold wherein the proportion of
161 sequencing reads derived from the mitochondrial genome was limited to less than 5%
162 (Supplementary Figure 9). Ultimately, 6051 endothelial cells were selected for further
163 analysis (Supplementary Figure 10, Supplementary Table 1).

164 Through clustering analysis of gene expression, these ECs were categorized into 6 clusters
165 using UMAP. These clusters include cluster 0, which consists of arterial and capillary ECs;
166 cluster1, comprising endocardium; cluster2, consisting of venous and lymphatic ECs;
167 cluster3, comprising arch ECs; cluster4, encompassing proliferating ECs; and cluster5,
168 consisting of vesicle enriched ECs (Figure 4b). The endothelial marker gene *cdh5* was
169 expressed in all the clusters (Figure 4c). The notch ligand *dlc* was highly expressed in
170 arterial, capillary ECs, and arch ECs (Figure 4d). The *dab2* and *prox1* were mainly enriched

171 in venous and lymphatic ECs (Figure 4e-f). The *cdk1*, which is a key player in cell cycle
172 regulation, was specifically expressed in proliferating ECs (Figure 4h). It was revealed that
173 the ratio of arterial and capillary ECs and proliferating ECs was increased in the high
174 glucose-treated embryos (Figure 4i, j), consistent with the observation that glucose treatment
175 resulted in excessive sprouting angiogenesis of ISVs.

176 **Foxo1a was significantly downregulated in arterial and capillary ECs**

177 To identify the potential molecules responsible for increasing the proportion of arterial and
178 capillary ECs in the embryos treated with glucose, we analyzed and compared the
179 differentially expressed genes (DEGs) in arterial and capillary ECs of control and glucose-
180 treated ECs. The results revealed that 1201 genes were up-regulated and 523 genes were
181 down-regulated significantly (Figure 5a). GO analysis revealed that these DEGs were
182 enriched in several biological processes, including regulation of actin filament organization,
183 blood vessel morphogenesis, development, angiogenesis, etc. (Figure 5b).

184 Subsequently, we searched for transcription factors among the genes involved in the
185 aforementioned biological processes that might participate in inducing excessive
186 angiogenesis. It has been reported that the loss of function of *foxo1a* led to excessive
187 angiogenesis [34, 35]. Our study also revealed that *foxo1a* was significantly downregulated in
188 arterial and capillary ECs after high glucose treatment compared to the ECs marker gene
189 *pecam1*(Figure 5c-e). The *in situ* hybridization (ISH) experiments further confirmed the
190 decrease in *foxo1a* expression following treatment with high D-glucose and L-glucose
191 (Figure 5f). To verify whether the downregulation of Foxo1a led to excessive angiogenesis in

192 zebrafish embryos, we performed loss-of-function experiments targeting *foxo1a*. AS1842856,
193 a cell-permeable inhibitor that has been reported to block *foxo1* transcription activity [36],
194 was administered to zebrafish embryos at 48 hpf and the imaging was performed at 72 hpf.
195 The results revealed significantly excessive angiogenesis in AS1842856 treated embryos
196 compared with the control group, consistent with the results obtained from *foxo1a* MO
197 injection (Figure 5g-i).

198 **Monosaccharides induced excessive angiogenesis through the *foxo1a-marcksl1a***
199 **pathway.**

200 A previous study has reported that *marcksl1a* overexpression in ECs in zebrafish led to a
201 significant increase in filopodia formation, similar to the phenotype we observed in response
202 to high glucose treatment [37]. Our analysis of the single-cell sequencing data revealed a
203 significant upregulation of *marcksl1a* in arterial and capillary ECs following high glucose
204 treatment, compared to the ECs marker gene *kdrl* (Figure 6a, b). The real-time qPCR and ISH
205 experiments further confirmed the elevated expression levels of *marccksl1a* following high
206 D-glucose and L-glucose treatment (Figure 6c, d). Then, by constructing the transgenic
207 zebrafish line *hsp70l:marcksl1a-p2A-mCherry:: Tg(fli1a:EGFP-CAAX)* ^{ntu666}, we conducted
208 the experiments to overexpress *marccksl1a* in zebrafish and subsequently observed the
209 vascular developmental phenotype. After one hour of heat shock for 1 hour at 24 hpf and
210 confocal imaging analysis at 72 hpf, significantly increased blood vessel formation was
211 observed in embryos overexpressing marccksl1a, compared with the control group (Figure
212 6e-g).

213 Given the results obtained from *marcksl1a* overexpression and loss of function of *foxo1a*,
214 we hypothesized that *marcksl1a* might be a target gene of Foxo1a. Therefore, we investigated
215 the impact of Foxo1 inhibition on marcksl1a expression in zebrafish embryos. As expected,
216 qPCR analysis revealed that inhibition of Foxo1 by AS1842856 resulted in upregulation of
217 *marcksl1a* expression (Figure 7a, b), which suggested that Foxo1a might negatively regulate
218 *marcksl1a* transcription in zebrafish. To further confirm it, we performed the Chromatin
219 Immunoprecipitation (ChIP) experiment to validate the potential binding interaction between
220 Foxo1 and *marcksl1a*. Since the amino acid sequence and DNA binding motifs of Foxo1 are
221 highly conserved between zebrafish and mice (Supplementary Figure 11), we analyzed the 3
222 kb promoter region of *marcksl1a* to search the binding site sequence of mouse FOXO1
223 presented in the JASPAR database. Two candidate binding sites (BS) were found at −265 to
224 −275 (BS1) and −153 to −163 (BS2) nucleotides upstream of the TSS of *marcksl1a* (Figure
225 7c) and then used for the ChIP-PCR assay detection. The results showed that Foxo1a was
226 enriched in both the predicted binding sites of *marcksl1a* (Figure 7d) in zebrafish.

227 Additionally, we microinjected *marcksl1a* MO into the 1-cell stage *Tg(fli1a:EGFP-CAAX)*
228 *ntu666* embryos, which were then treated with high levels of D-glucose and L-glucose. The
229 findings revealed that the knockdown of Marcksl1a could effectively mitigate the excessive
230 angiogenesis caused by high D-glucose or high L-glucose treatment, resembling the rescue
231 effect observed with VEGFR inhibitor lenvatinib (Figure 7e-k, Supplementary Figure 11).
232 These results suggested that monosaccharides induced excessive angiogenesis through the
233 Foxo1a-*marcksl1a* pathway in zebrafish embryos.

Discussion

In this study, we successfully established a new zebrafish model with significant excessive angiogenesis, resembling the hyperangiogenic characteristics observed in PDR more closely than previously established models [30, 32]. Seung-Hyun Jung et al. have described a short-term zebrafish model for diabetic retinopathy (DR) induced by high glucose, which exhibited blood vessel defects[30]. However, these defects were limited to the disruption of tight junctions and dilation of hyaloid-retinal vessels [30], without the excessive angiogenesis and vascular blockage observed in PDR and our established model. Additionally, although Kristina Jörgens et al. have observed the hyperbranching of small vessel structures originating from the upper part of ISVs, growing horizontally towards and partially connecting to the neighboring ISVs Field [32], the angiogenic sprouts did not form a more complex structure that was observed in our research.

The excessive development of immature blood vessels represents a significant pathological condition in the progression of DR and nephropathy [38, 39]. Hyperglycemia has been considered one of the most causal factors causing vascular damage, including excessive angiogenesis. However, the exact mechanism through which hyperglycemia impairs the blood vessels is not well determined. To gain more insights into it, we performed the analysis of single-cell transcriptomic sequencing data of the endothelial cells isolated from D-glucose-treated embryos. The findings revealed an increased ratio of tip cells and proliferating ECs, accompanied by the altered expression of various angiogenic genes in the ECs of D-glucose-treated embryos.

256 Foxo1 has been validated to be essential for sustaining the quiescence of endothelial cells,
257 with involvement in metabolism regulation [34, 40]. Moreover, it also plays important roles
258 in diabetic microvascular complications including DR[41, 42]. Here, by combining the
259 single-cell transcriptomic sequencing data analysis and experimental validation, we identified
260 the transcription factor Foxo1a, which was significantly down-regulated in the embryos
261 treated with high glucose, responsible for the excessive angiogenesis. Additionally, our result
262 further revealed that Foxo1a exerts its regulatory function during this process by down-
263 regulating its target gene *marcksl1a*, regardless of whether the embryos were treated with D-
264 glucose or L-glucose. Taken together, our results suggested that both caloric and noncaloric
265 monosaccharides treatment could lead to excessive angiogenesis by promoting the
266 differentiation of quiescent endothelial cells into tip cells through the *foxo1a-marcksl1a*
267 pathway.

268 The consumption of ASB has been linked to the occurrence and development of
269 cardiovascular disease in previous studies [12, 16-23]. However, the potential mechanisms
270 underlying the association have not been well documented. In recent years, positive
271 associations between ASB and cardiovascular disease have been proposed, possibly due to
272 several plausible factors, including the potential impact of ASBs on central nervous system
273 circuits, gut hormone secretion, and gut microbiota [43-45]. Additionally, it has been
274 hypothesized that the ASBs might stimulate appetite and increase calorie intake [43, 44].

275 For a long time, there has been considerable debate and conflicting opinions regarding how
276 specific sugars affect the development of type 2 diabetes rather than excess calories per se

277 [46, 47]. In this study, we have provided new evidence indicating that the administration of
278 noncaloric monosaccharides leads to significant excessive angiogenesis, suggesting that the
279 excessive angiogenesis may not be only attributed to the caloric properties. Since excessive
280 angiogenesis is the major pathological feature of diabetic retinopathy and nephropathy, our
281 findings are in support of a possible biological mechanism underlying the positive
282 associations between noncaloric monosaccharides and microvascular complications
283 associated with type 2 diabetes, suggesting that the noncaloric monosaccharides might not be
284 suitable for ASB consumption.

285 Surprisingly, no notable abnormalities were observed in the vessels of embryos treated
286 with disaccharides, including lactose, maltose, and sucrose, which is consistent with the
287 previous study stating that intakes of sucrose, lactose, and maltose were not significantly
288 associated with the risk of type 2 diabetes [48]. This finding implied that the effects induced
289 by monosaccharides cannot be attributed to the osmotic pressure of the surrounding medium.
290 Furthermore, despite the potential conversion of these disaccharides into monosaccharides,
291 the restricted reaction rate may maintain them within a safe concentration range that is not
292 harmful to the vessels in a short period.

293 In conclusion, to investigate the effects of monosaccharides on vascular development, we
294 established a zebrafish model by treating the embryos with high concentrations of
295 monosaccharides. Based on this model, we observed significant excessive angiogenesis
296 induced by glucose and noncaloric monosaccharides, initiated by activating the quiescent
297 endothelial cells into proliferating tip cells. The effects of monosaccharides on inducing

298 excessive angiogenesis were then proved to be mediated by the *foxo1a-marcksl1a* pathway.
299 The results have provided novel insights into the roles of noncaloric monosaccharides in
300 human health and the underlying mechanisms.

301 **Materials and methods**

302 **Zebrafish**

303 Care and breeding of zebrafish were carried out as previously described [49]. Animal
304 experiments were conducted according to local institutional laws and Chinese law for the
305 Protection of Animals. The following transgenic strains were used: *Tg(fli1aEP:EGFP-*
306 *CAAX)*^{ntu666} and *Tg(kdrl:ras-mCHerry* [33]. Embryos were obtained through natural mating
307 and maintained at 28.5°C. The stages of zebrafish embryos are defined as previously
308 described [49]. Embryos were treated with 0.2 mM 1-phenyl-2-thiourea (PTU, Sigma,
309 P7629) to block pigmentation for further imaging analysis.

310 **Monosaccharides and drug treatment**

311 The D-glucose (Sigma, G7021-100g), L-glucose (Sigma, G5500-1g; J&K, 981195-1g), D-
312 Fructose (Sigma, F0127-100g), L-Rhamnose monohydrate (Aladdin, R108982), D-Sorbitol
313 (Sigma, S1876-100g), D-Mannitol (Sigma, M4125-100g), D-(-)-Ribose (Sigma, V900389-
314 25g), L-(+)-Arabinos (Sigma, V900920-25g), Mannose (Sigma, M2069-25g) and sucrose
315 (Sigma, V900116-500G) were dissolved in E3 solution. Zebrafish embryos at 24 hpf to 48
316 hpf were placed in 24-well plates (ten embryos per well) and immersed in the solution at the
317 presetting concentrations and time windows. Then, put it in a 28 ℃ incubator for cultivation.
318 Five days before embryonic development, a stereo fluorescence microscope and a laser

319 confocal microscope were used to observe the changes in blood vessel phenotype. For the
320 drug treatment, the embryos were co-incubated in glucose with lenvatinib (Selleck, S1164-
321 5MG) from 48 hpf to 96 hpf. Foxo1 inhibitor AS1842856 (MCE, HY-100596) was dissolved
322 in DMSO and stored at -80℃ and diluted with E3 solution when used. The same
323 concentration of DMSO was used as a negative control.

324 **Glucose concentration measurement**

325 Glucose concentration in the embryo was measured as described previously [50]. Embryos
326 that developed to 75% epiboly were selected and transferred to 24-well plates (ten embryos
327 per well) and immersed in the solution at the presetting concentrations and time windows.
328 For glucose concentration measurement, embryos (n=20) were transferred to a new 1.5 mL
329 tube, rinsed three times with 1×PBS, and immersed in ice for the following experiments.
330 Discard the PBS as much as possible, embryos homogenized using a hand homogenizer, and
331 centrifuged at 14,000×g for 10 min. 1.5 μL of the supernatant was used to measure the total
332 free-glucose level using a glucometer (Baye, 7600P).

333 **Whole-mount in situ hybridization (WISH)**

334 Whole-mount in situ hybridization and the preparation of antisense RNA probes were
335 performed as described in the previous protocol [51]. Briefly, the *marcksl1a* and *foxo1a*
336 cDNA fragments were cloned with the specific primers listed below using the wild-type
337 embryo (AB) cDNA library. Probes were synthesized using the in vitro DIG-RNA labeling
338 transcription Kit (Roche, 11175025910) with linearized pGEM-T easy vector containing
339 *marcksl1a* or *foxo1a* gene fragment as the templates. Synthesized probes were purified with

340 LiCl (Invitrogen, AM9480) and diluted to 1 ng/μL for hybridization. Zebrafish embryos were
341 collected and fixed with 4% paraformaldehyde (PFA) overnight at 4˚C, then dehydrated with
342 methanol gradients and stored at -20℃ in 100% methanol. The hybridization result was
343 detected with anti-DIG-AP antibody (1:2000, Roche, 11093274910) and NBT/BCIP (1:500,
344 Roche, 11681451001). After hybridization, images of the embryos were captured with an
345 Olympus stereomicroscope MVX10. The primers are listed below:
346 *marcksl1a*-probe-forward:5'- AGG ATG GGT GCT CAG TTG AC-3'
347 *marcksl1a*-probe-reverse:5'- GCT GGC GTC TCA TTG GTT TC-3'
348 *foxo1a*-probe-forward:5'-GCA ACA CAG GAT TTC CCC AC-3'
349 *foxo1a*-probe-reverse:5'-CAC AGG TGG CAC TGG AAG G-3'

350 **Single-cell gene expression profile analysis**

351 Cell Ranger 3.0.2 (https://github.com/10XGenomics/cellranger) was used to convert the
352 raw sequencing data to a single-cell level gene count matrix. The clustering of single cells
353 and the marker genes in each cluster were analyzed by Seurat 3.0
354 (https://satijalab.org/seurat/install.html) [52]. Several criteria were applied to select the single
355 cells, including only keeping the genes that are expressed (Unique Molecular Identifiers or
356 UMI larger than 0) at least in 3 single cells, selecting single cells with the number of
357 expressed genes at the range between 500 and 3000, and requiring the percentage of
358 sequencing reads on mitochondrial genome being less than 5 percentage. Furthermore,
359 sctransform method [53] was applied to remove technical variation, and ClusterProfiler [54]
360 was used to do the Gene Ontology enrichment analysis based on the marker genes of each

361 cell cluster. Detailed information about the data processing can be found in the source code of
362 this project (https://github.com/gangcai/ZebEndoimmune).

363 **Gene expression analysis by quantitative real-time PCR**

364 Total RNA was extracted from zebrafish embryos using TRIzol™ (Invitrogen, 15596026),
365 and stored at -80°C. The cDNA was then synthesized using the HiScript II Q RT SuperMix
366 for qPCR Kit (Vazyme, R223-01) according to the manufacturer's instructions. Quantitative
367 PCR was performed in triplicates using the Taq Pro Universal SYBR qPCR Master Mix
368 (Vazyme, Q712-02) on a real-time PCR detection system (StepOne™ Real-Time PCR
369 Systems). The primers used for Real-time PCR analysis are as follows:
370 ef1α-Qpcr-F:5'- CTT CAA CGC TCA GGT CAT CA -3'
371 ef1α-Qpcr-R:5'- CGG TCG ATC TTC TCC TTG AG -3
372 marcksl1a-Qpcr-F:5'- CCG TGG CTG ATA AAG CCA AT -3'
373 marcksl1a-Qpcr-R:5'- CTC CCT CCT CCG TTT TTG GG -3'

374 **Transgenic and heat shock**

375 The *Tg(fli1aEP:EGFP-CAAX)*^{ntu666} line was established using a construct *fli1aEP:EGFP-*
376 *CAAX*, which was generated using multisite Gateway technology, the tol2 kit as previously
377 described [55]. The 5' Entry p5Efli1ep (#31160) purchased from Addgene was originally
378 from Nathan Lawson Lab [56]. Three entry clones and the pDestTol2pA2 destination vector
379 were used to generate the expression construct by LR recombination reaction as described in
380 the Multisite Gateway Manual book. The expression constructs were synthesized by
381 GENEWIZ company. The zebrafish embryos were immersed in a 37 °C water bath for 1 hour

382 for heat shock. Around 75 pg of expression plasmid DNA and 25 pg tol2 transposase mRNA
383 were premixed and microinjected into single-cell fertilized eggs.

384 **Chip-PCR**

385 Embryos injected with *hsp70l:foxo1a-6×His-P2A-mCherry* were collected at 72 hpf after
386 heat shock treatment. According to the manufacturer's instructions, the ChIP-PCR assay was
387 performed using the Chromatin Immunoprecipitation (ChIP) Assay Kit (Millipore, 3753379).
388 The genomic DNA crossed with Foxo1a protein was immunoprecipitated by using 5 μg Anti-
389 6×His tag antibody (abcam, ab213204). Antibody against lgG was used as a negative control.
390 The semiquantitative PCR was performed with KODfx (TOYOBO, KFX-101) at the
391 following conditions: 94℃ for 5 min; 35 cycles of 98℃ for 10 s, 55℃ for 30 s, 68℃ for 10
392 s; 68℃ for 10 min. The PCR primers used for the predicted binding sites (BS) are as follows:
393 Marcksl1a-BS1-forward:5'- CCC TTT TTC AAA AGT GAG TTT GAG -3'
394 Marcksl1a -BS1-reverse:5'- GGA GCT TCA TCT GCC CCA TT -3'
395 Marcksl1a -BS2-forward:5'- CGG TTT CCA GCT TTC TTC AGA A -3'
396 Marcksl1a -BS2-reverse:5'- TCT CAA ACT CAC TTT TGA AAA AGG G -3'

397 **Imaging analysis**

398 For confocal imaging of blood vessels in fluorescence protein labeled transgenic zebrafish
399 embryos, they were anesthetized with egg water/0.16 mg/mL MS222 (Sigma, A5040)/1%
400 PTU and embedded in 0.5-0.8% low melting agarose. Confocal imaging was performed with
401 a Nikon A1R HD25 Confocal Microscope. Analysis was performed using Nikon-NIS-
402 Elements software. The bright field images were acquired with an Olympus DP71 camera on

403 an Olympus stereomicroscope MVX10.

404 **Statistical analysis**

405 Statistical analysis was performed with a student's t-test. All data is presented as Mean ±
406 SEM; $p < 0.05$ was considered statistically significant.

407 **Funding**

408 This study was supported by grants from the National Natural Science Foundation of
409 China (81870359, 2018YFA0801004).

410 **Conflicts of interest/Competing interests**

411 The authors declare that they have no conflicts of interest

412 **Availability of data and material (data transparency)**

413 All the experimental materials generated in this study are available from the corresponding
414 authors upon reasonable request.

415 **Authors' contributions**

416 Dong Liu, Xuchu Duan, Xia Liu, and Gangcai Xie conceived and designed the
417 experiments and wrote the manuscript. Xiaoning wang, Jinxiang Zhao, Jiehuan Xu, Bowen
418 Li, and Gangcai Xie performed the experiments and analyzed the data. All authors read and
419 approved the final manuscript.

420 **Ethics approval**

421 All zebrafish experimentation was carried out following the NIH Guidelines for the care
422 and use of laboratory animals (http://oacu.od.nih.gov/regs/index.htm) and ethically approved

by the Administration Committee of Experimental Animals, Jiangsu Province, China (Approval ID: 20180905-002).

Acknowledgments

Not applicable

427 **Reference**

428 1. Matheus, A.S., et al., *Impact of diabetes on cardiovascular disease: an update.*
429 Int J Hypertens, 2013. **2013**: p. 653789.
430 2. Fox, C.S., et al., *Trends in cardiovascular complications of diabetes.* JAMA,
431 2004. **292**(20): p. 2495-9.
432 3. Rask-Madsen, C. and G.L. King, *Vascular complications of diabetes:*
433 *mechanisms of injury and protective factors.* Cell Metab, 2013. **17**(1): p. 20-33.
434 4. Flammer, A.J., et al., *The assessment of endothelial function: from research*
435 *into clinical practice.* Circulation, 2012. **126**(6): p. 753-67.
436 5. Kolluru, G.K., S.C. Bir, and C.G. Kevil, *Endothelial dysfunction and diabetes:*
437 *effects on angiogenesis, vascular remodeling, and wound healing.* Int J Vasc
438 Med, 2012. **2012**: p. 918267.
439 6. Tesfamariam, B., et al., *Elevated glucose promotes generation of*
440 *endothelium-derived vasoconstrictor prostanoids in rabbit aorta.* J Clin Invest,
441 1990. **85**(3): p. 929-32.
442 7. Ting, H.H., et al., *Vitamin C improves endothelium-dependent vasodilation in*
443 *patients with non-insulin-dependent diabetes mellitus.* J Clin Invest, 1996.
444 **97**(1): p. 22-8.
445 8. Imamura, F., et al., *Consumption of sugar sweetened beverages, artificially*
446 *sweetened beverages, and fruit juice and incidence of type 2 diabetes:*
447 *systematic review, meta-analysis, and estimation of population attributable*
448 *fraction.* BMJ, 2015. **351**: p. h3576.
449 9. Malik, V.S., *Sugar sweetened beverages and cardiometabolic health.* Curr
450 Opin Cardiol, 2017. **32**(5): p. 572-579.
451 10. Narain, A., C.S. Kwok, and M.A. Mamas, *Soft drinks and sweetened*
452 *beverages and the risk of cardiovascular disease and mortality: a systematic*
453 *review and meta-analysis.* Int J Clin Pract, 2016. **70**(10): p. 791-805.
454 11. Larsson, S.C., A. Akesson, and A. Wolk, *Sweetened beverage consumption is*
455 *associated with increased risk of stroke in women and men.* J Nutr, 2014.
456 **144**(6): p. 856-60.
457 12. Fung, T.T., et al., *Sweetened beverage consumption and risk of coronary*
458 *heart disease in women.* Am J Clin Nutr, 2009. **89**(4): p. 1037-42.

13. Fakhouri, T.H., B.K. Kit, and C.L. Ogden, *Consumption of diet drinks in the United States, 20092010.* NCHS Data Brief, 2012(109): p. 1-8.
14. Sylvetsky, A.C., et al., *Low-calorie sweetener consumption is increasing in the United States.* Am J Clin Nutr, 2012. **96**(3): p. 640-6.
15. Moriconi, E., et al., *Neuroendocrine and Metabolic Effects of Low-Calorie and Non-Calorie Sweeteners.* Front Endocrinol (Lausanne), 2020. **11**: p. 444.
16. de Koning, L., et al., *Sweetened beverage consumption, incident coronary heart disease, and biomarkers of risk in men.* Circulation, 2012. **125**(14): p. 1735-41, S1.
17. Fagherazzi, G., et al., *Consumption of artificially and sugar-sweetened beverages and incident type 2 diabetes in the Etude Epidemiologique aupres des femmes de la Mutuelle Generale de l'Education Nationale-European Prospective Investigation into Cancer and Nutrition cohort.* Am J Clin Nutr, 2013. **97**(3): p. 517-23.
18. Gardener, H., et al., *Diet soft drink consumption is associated with an increased risk of vascular events in the Northern Manhattan Study.* J Gen Intern Med, 2012. **27**(9): p. 1120-6.
19. Drouin-Chartier, J.P., et al., *Changes in Consumption of Sugary Beverages and Artificially Sweetened Beverages and Subsequent Risk of Type 2 Diabetes: Results From Three Large Prospective U.S. Cohorts of Women and Men.* Diabetes Care, 2019. **42**(12): p. 2181-2189.
20. de Koning, L., et al., *Sugar-sweetened and artificially sweetened beverage consumption and risk of type 2 diabetes in men.* Am J Clin Nutr, 2011. **93**(6): p. 1321-7.
21. Hirahatake, K.M., et al., *Cumulative intake of artificially sweetened and sugar-sweetened beverages and risk of incident type 2 diabetes in young adults: the Coronary Artery Risk Development In Young Adults (CARDIA) Study.* Am J Clin Nutr, 2019. **110**(3): p. 733-741.
22. Mossavar-Rahmani, Y., et al., *Artificially Sweetened Beverages and Stroke, Coronary Heart Disease, and All-Cause Mortality in the Women's Health Initiative.* Stroke, 2019. **50**(3): p. 555-562.
23. Vyas, A., et al., *Diet drink consumption and the risk of cardiovascular events: a report from the Women's Health Initiative.* J Gen Intern Med, 2015. **30**(4): p.

492 462-8.
493 24. Zang, L., L.A. Maddison, and W. Chen, *Zebrafish as a Model for Obesity and*
494 *Diabetes.* Front Cell Dev Biol, 2018. **6**: p. 91.
495 25. Barros, T.P., et al., *Zebrafish: an emerging technology for in vivo*
496 *pharmacological assessment to identify potential safety liabilities in early drug*
497 *discovery.* Br J Pharmacol, 2008. **154**(7): p. 1400-13.
498 26. Elo, B., et al., *Larval zebrafish as a model for glucose metabolism: expression*
499 *of phosphoenolpyruvate carboxykinase as a marker for exposure to anti-*
500 *diabetic compounds.* J Mol Endocrinol, 2007. **38**(4): p. 433-40.
501 27. Gleeson, M., V. Connaughton, and L.S. Arneson, *Induction of hyperglycaemia*
502 *in zebrafish (Danio rerio) leads to morphological changes in the retina.* Acta
503 Diabetol, 2007. **44**(3): p. 157-63.
504 28. Alvarez, Y., et al., *Predominant cone photoreceptor dysfunction in a*
505 *hyperglycaemic model of non-proliferative diabetic retinopathy.* Dis Model
506 Mech, 2010. **3**(3-4): p. 236-45.
507 29. Jorgens, K., et al., *Zebrafish: a model for understanding diabetic*
508 *complications.* Exp Clin Endocrinol Diabetes, 2012. **120**(4): p. 186-7.
509 30. Jung, S.H., et al., *High glucose-induced changes in hyaloid-retinal vessels*
510 *during early ocular development of zebrafish: a short-term animal model of*
511 *diabetic retinopathy.* Br J Pharmacol, 2016. **173**(1): p. 15-26.
512 31. Heckler, K. and J. Kroll, *Zebrafish as a Model for the Study of Microvascular*
513 *Complications of Diabetes and Their Mechanisms.* Int J Mol Sci, 2017. **18**(9).
514 32. Jorgens, K., et al., *High tissue glucose alters intersomitic blood vessels in*
515 *zebrafish via methylglyoxal targeting the VEGF receptor signaling cascade.*
516 Diabetes, 2015. **64**(1): p. 213-25.
517 33. Krueger, J., et al., *Flt1 acts as a negative regulator of tip cell formation and*
518 *branching morphogenesis in the zebrafish embryo.* Development, 2011.
519 **138**(10): p. 2111-20.
520 34. Wilhelm, K., et al., *FOXO1 couples metabolic activity and growth state in the*
521 *vascular endothelium.* Nature, 2016. **529**(7585): p. 216-20.
522 35. Rudnicki, M., et al., *Endothelial-specific FoxO1 depletion prevents obesity-*
523 *related disorders by increasing vascular metabolism and growth.* Elife, 2018.
524 **7**.

525 36. Zhao, W., et al., *Endothelial CDS2 deficiency causes VEGFA-mediated*
526 *vascular regression and tumor inhibition.* Cell Res, 2019. **29**(11): p. 895-910.
527 37. Kondrychyn, I., et al., *Marcksl1 modulates endothelial cell mechanoresponse*
528 *to haemodynamic forces to control blood vessel shape and size.* Nature
529 Communications, 2020. **11**(1): p. 5476.
530 38. Wilkinson-Berka, J.L., *Vasoactive factors and diabetic retinopathy: vascular*
531 *endothelial growth factor, cycoloxygenase-2 and nitric oxide.* Curr Pharm Des,
532 2004. **10**(27): p. 3331-48.
533 39. Osterby, R. and G. Nyberg, *New vessel formation in the renal corpuscles in*
534 *advanced diabetic glomerulopathy.* J Diabet Complications, 1987. **1**(4): p.
535 122-7.
536 40. Andrade, J., et al., *Control of endothelial quiescence by FOXO-regulated*
537 *metabolites.* Nat Cell Biol, 2021. **23**(4): p. 413-423.
538 41. Parmar, U.M., et al., *Emerging links between FOXOs and diabetic*
539 *complications.* Eur J Pharmacol, 2023. **960**: p. 176089.
540 42. Behl, T., et al., *Mechanistic insights into the role of FOXO in diabetic*
541 *retinopathy.* Am J Transl Res, 2022. **14**(6): p. 3584-3602.
542 43. Blundell, J.E. and A.J. Hill, *Paradoxical effects of an intense sweetener*
543 *(aspartame) on appetite.* Lancet, 1986. **1**(8489): p. 1092-3.
544 44. Pepino, M.Y., *Metabolic effects of non-nutritive sweeteners.* Physiol Behav,
545 2015. **152**(Pt B): p. 450-5.
546 45. Nettleton, J.E., R.A. Reimer, and J. Shearer, *Reshaping the gut microbiota:*
547 *Impact of low calorie sweeteners and the link to insulin resistance?* Physiol
548 Behav, 2016. **164**(Pt B): p. 488-493.
549 46. Qi, X. and R.F. Tester, *Lactose, Maltose, and Sucrose in Health and Disease.*
550 Mol Nutr Food Res, 2020. **64**(8): p. e1901082.
551 47. Laville, M. and J.A. Nazare, *Diabetes, insulin resistance and sugars.* Obes
552 Rev, 2009. **10 Suppl 1**: p. 24-33.
553 48. Montonen, J., et al., *Consumption of Sweetened Beverages and Intakes of*
554 *Fructose and Glucose Predict Type 2 Diabetes Occurrence1.* The Journal of
555 Nutrition, 2007. **137**(6): p. 1447-1454.
556 49. Wang, X., et al., *MicroRNA-10a/10b represses a novel target gene mib1 to*
557 *regulate angiogenesis.* Cardiovasc Res, 2016. **110**(1): p. 140-50.

558 50. Da'as, S.I., et al., *The link between glycemic control measures and eye*
559 *microvascular complications in a clinical cohort of type 2 diabetes with*
560 *microRNA-223-3p signature.* J Transl Med, 2023. **21**(1): p. 171.
561 51. Huang, Y., et al., *Nonmuscle myosin II-B (myh10) expression analysis during*
562 *zebrafish embryonic development.* Gene Expr Patterns, 2013. **13**(7): p. 265-
563 270.
564 52. Butler, A., et al., *Integrating single-cell transcriptomic data across different*
565 *conditions, technologies, and species.* Nat Biotechnol, 2018. **36**(5): p. 411-
566 420.
567 53. Hafemeister, C. and R. Satija, *Normalization and variance stabilization of*
568 *single-cell RNA-seq data using regularized negative binomial regression.*
569 Genome Biol, 2019. **20**(1): p. 296.
570 54. Yu, G., et al., *clusterProfiler: an R package for comparing biological themes*
571 *among gene clusters.* OMICS, 2012. **16**(5): p. 284-7.
572 55. Kwan, K.M., et al., *The Tol2kit: a multisite gateway-based construction kit for*
573 *Tol2 transposon transgenesis constructs.* Dev Dyn, 2007. **236**(11): p. 3088-99.
574 56. Villefranc, J.A., J. Amigo, and N.D. Lawson, *Gateway compatible vectors for*
575 *analysis of gene function in the zebrafish.* Dev Dyn, 2007. **236**(11): p. 3077-87.

576

577

578 **Figure Legends**

579 **Figure 1 Glucose treatment caused excessive angiogenesis in zebrafish. a**, A diagram
580 showing the glucose treatment time window and imaging time point. **b**, A diagram indicating
581 the imaging positions of the zebrafish embryos. **c**, Confocal imaging analysis of the control
582 and glucose-treated embryos. The red bar indicates position 1; the green bar indicates
583 position 2. Arrowheads indicate the ectopic branching from the dorsal aorta. Stars indicate the
584 ectopic vessels from ISVs and DLAVs. **d**, Statistical analysis of the total length of ISVs in
585 control and glucose-treated embryos. t-test, ****$p<0.0001$. **e**, A diagram showing the glucose
586 treatment time window and imaging time point. **f**, Confocal imaging analysis of the control
587 and glucose-treated embryos. The red bar indicates position 1; the green bar indicates
588 position 2. Arrowheads indicate the ectopic branching from the dorsal aorta. Stars indicate the
589 ectopic vessels from ISVs and DLAVs. **g**, Statistical analysis of the total length of ISVs in
590 control and glucose-treated embryos. t-test, ****$p<0.0001$. **h**, A diagram showing the glucose
591 treatment time window and imaging time point. **i**, Confocal imaging analysis of the control
592 and glucose-treated embryos. The red bar indicates position 1; the green bar indicates
593 position 2. Arrowheads indicate the ectopic branching from the dorsal aorta. Stars indicate the
594 ectopic vessels from ISVs and DLAVs. **j**, Statistical analysis of the total length of ISVs in
595 control and glucose-treated embryos. t-test, ****$p<0.0001$. **k**, A diagram showing the glucose
596 treatment time window and imaging time point. **l**, Confocal imaging analysis of the control
597 and glucose-treated embryos. The red bar indicates position 1; the green bar indicates
598 position 2. Arrowheads indicate the ectopic branching from the dorsal aorta. Stars indicate the
599 ectopic vessels from ISVs and DLAVs. **m**, Statistical analysis of the total length of ISVs in

600 control and glucose-treated embryos. t-test, ****p<0.0001. **o**, A diagram showing the blood
601 vessels in position 2 indicated in panel b of control embryos. **p**, A diagram showing the blood
602 vessels in position 2 indicated in panel b of high glucose-treated embryos.
603
604 **Figure 2 L-glucose and mannose treatment caused excessive angiogenesis as well. a,** A
605 diagram showing the monosaccharides treatment time window and imaging time point. **b**, A
606 diagram indicating the imaging position of the zebrafish embryos. **c-g**, Confocal imaging
607 analysis of the control and monosaccharides, including L-glucose, D-mannose, D-ribose, and
608 L-arabinose, treated embryos. Arrowheads indicate the ectopic branching from the dorsal
609 aorta. Stars indicate the ectopic vessels from ISVs. **h**, Statistical analysis of the total length of
610 ISVs in control and monosaccharides treated embryos. t-test, ****p<0.0001.
611
612 **Figure 3 High glucose treatment induced endothelial differentiation into tip cell-like**
613 **cells. a,** A diagram showing the confocal time-lapse imaging time window. **b**, A diagram
614 indicating the imaging position of the zebrafish embryos. c, Confocal time-lapse imaging
615 analysis of blood vessels in control *Tg(fli1aEP:EGFP-CAAX)*^{ntu666} embryos. **d**, A diagram
616 showing the glucose treatment time window and confocal time-lapse imaging time window.
617 **e**, Confocal time-lapse imaging analysis of blood vessels in glucose-treated
618 *Tg(fli1aEP:EGFP-CAAX)*^{ntu666} embryos. Arrowheads indicate the ectopic angiogenic
619 branches. **f**, A snapshot of confocal time-lapse imaging analysis of blood vessels in glucose-
620 treated *Tg(fli1aEP:EGFP-CAAX)*^{ntu666} embryos. Z stacks were used to make 3D color
621 projections, where blue represents the most proximal (closest to the viewer), and red

622 represents the most distal (farthest from the viewer). Arrowheads indicate ectopic angiogenic
623 sprouts. **g**, A snapshot of confocal time-lapse imaging analysis of an ISV in glucose-treated
624 *Tg(fli1aEP:EGFP-CAAX)*^{ntu666} embryos. Arrowheads indicate ectopic angiogenic sprouts.
625
626 **Figure 4 Single-cell transcriptome sequencing analysis of endothelial cells in control and**
627 **high glucose treated embryos. a**, Schematic diagram of the single-cell sequencing process.
628 300 embryos in the control group and 300 embryos in the high glucose group were used, and
629 ECs were sorted by GFP fluorescent using FACS technology. **b**, The measured cells were
630 divided into 6 individual clusters based on gene expression profiles using UMAP. **c-h**, The
631 violin plots of some endothelial cell marker genes. **i**, The proportion of ECs in each cluster of
632 the control and high glucose groups. **j**, Changes of ECs percentage in arterial and capillary
633 ECs, endocardium, and proliferating ECs of control and high glucose group.
634
635 **Figure 5 Foxo1a was involved in the excessive angiogenesis induced by high glucose**
636 **treatment. a**, The volcano plot of differential expression genes in arterial and capillary ECs.
637 The avg_log2FC greater than 1 was considered significant, including 523 down-regulated
638 genes (blue dots) and 1201 up-regulated genes (red dots). **b**, GO analysis of 523 down-
639 regulated genes in arterial and capillary ECs. **c,** The feature plot of ECs marker gene pecam1
640 of control and high glucose group in arterial and capillary ECs. **c',** The violin plot of ECs
641 marker gene pecam1 of control and high glucose group in arterial and capillary ECs. **d**, The
642 feature plot of gene foxo1a of control and high glucose group in arterial and capillary ECs.
643 **d',** The violin plot of gene foxo1a of control and high glucose group in arterial and capillary

644 ECs. **e**, Average expression of gene pecam1 and foxo1a in control and high glucose group. **f**,
645 Whole-mount in situ hybridization analysis of foxo1a in control, high glucose, and high L-
646 glucose treated embryos. **g**, A diagram showing the foxo1 inhibitor treatment time window. **h**,
647 Confocal imaging analysis of control embryos, AS1842856 treated embryos, and foxo1a MO-
648 injected embryos. **i**, Statistical analysis of the total length of ISVs in control embryos,
649 AS1842856 treated embryos, and foxo1a MO-injected embryos. *t-test*, ****$p<0.0001$.
650
651 **Figure 6 Marcksl1a over-expression induced excessive angiogenesis in zebrafish**
652 **embryos. a**, The violin plot of ECs marker gene kdrl of control and high glucose group in
653 arterial and capillary ECs. **b**, The violin plot of gene marcksl1a of control and high glucose
654 group in arterial and capillary ECs. **c,** Real-rime PCR analysis of marcksla1a expression in
655 control, high glucose, and high L-glucose treated embryos. *t-test*, ****$p<0.0001$. **d**, Whole-
656 mount in situ hybridization analysis of mmarcksl1a in control, high glucose, and high L-
657 glucose treated embryos. **e-f'**, Confocal imaging analysis of blood vessels in control and
658 *hsp70l:marcksl1a-P2A-mCherry* injected *Tg(fli1aEP:EGFP-CAAX)*^{ntu666} embryos. **g**,
659 Statistical analysis of the total length of ISVs in control and *hsp70l:marcksl1a-P2A-mCherry*
660 injected embryos. *t-test*, **$p<0.01$.
661
662 **Figure 7 Noncaloric monosaccharides induced excessive angiogenesis through foxo1a-**
663 **marcksl1a signal in zebrafish embryos. a**, A diagram showing the Foxo1 inhibitor
664 treatment time window. **b**, Real-rime PCR analysis of marcksla1a expression in control and
665 AS1842856 treated embryos. Two-way ANOVA, **$p<0.01$, ***$p<0.001$. **c**, A sequence logo

666 of Foxo1 binding sequence presented in JASPAR database (https://jaspar.genereg.net/) and
667 two candidate binding sites at the upstream of transcription start site (TSS) of mmarcksl1a in
668 zebrafish. **d**, Results of the ChIP-PCR assay indicated that BS1 and BS2 are Foxo1a-binding
669 sites of marcksl1a in zebrafish. Input sonicated genomic DNA samples without
670 immunoprecipitation as a positive control. IgG, sonicated, and IgG-immunoprecipitated
671 genomic DNA samples as a negative control. **e-j**, Confocal imaging analysis of blood vessels
672 in control, high glucose, high glucose & Lenvatinib, high glucose+marcksl1a MO, high L-
673 glucose and high L-glucose+marcksl1a MO groups. **k**, Statistical analysis of the total length
674 of ISVs in the groups in figure e-j, respectively. one-way ANOVA, ****$p<0.0001$.
675
676
677
678
679

Supplementary Figure Legends

Supplementary Figure 1 Confocal imaging analysis of *Tg(fli1aEP:EGFP-CAAX)^{ntu666}* embryos at 48 hpf (a) and 3 dpf (b).

Supplementary Figure 2 The diagrams show the glucose treatment time window and imaging time point.

Supplementary Figure 3 Total glucose concentrations at different development stages in control and high glucose treated embryos. **a**, A diagram showing the glucose treatment time window and concentration measuring time point. **b**, Statistical analysis of the glucose concentration in control and high glucose-treated embryos. one-way ANOVA, ****$p<0.0001$.

Supplementary Figure 4 Stereo microscopic analysis of control, glucose, and sucrase-treated embryos in a bright field. a-c, Imaging analysis of control, glucose, and sucrase treated embryos in bright field. **d**, A diagram showing the sucrase treatment time window and imaging time point. **e**, A diagram indicating the imaging positions of the zebrafish embryos. **f,** Confocal imaging analysis of the control and sucrase treated *Tg(fli1aEP:EGFP-CAAX)^{ntu666}* embryos. The red bar indicates position 1; the green bar indicates the position. **g**, A diagram showing the sucrase treatment time window and imaging time point. **h**, Confocal imaging analysis of the control and sucrase treated *Tg(fli1aEP:EGFP-CAAX)^{ntu666}* embryos. The red bar indicates position 1; the green bar indicates the position.

702

703 **Supplementary Figure 5 Confocal imaging analysis of 1% - 4% glucose treated blood**
704 **vessels. a**, A diagram showing the glucose treatment time window and imaging time point. **b-**
705 **g'**, Confocal imaging analysis of the control, 1%, 2%, 3%, and 4% glucose-treated
706 *Tg(fli1aEP:EGFP-CAAX)*^{ntu666} embryos.

707

708 **Supplementary Figure 6 Fructose treatment caused excessive angiogenesis in zebrafish.**
709 **a**, A diagram showing the fructose treatment time window and imaging time point. **b**, A
710 diagram indicating the imaging position of the zebrafish embryos. **c-d**, Confocal imaging
711 analysis of the control and glucose-treated *Tg(fli1aEP:EGFP-CAAX)*^{ntu666} embryos. e-f,
712 Imaging analysis of control and fructose treated embryos in bright field.

713

714 **Supplementary Figure 7 Lactose and maltose treatment did not cause excessive**
715 **angiogenesis in zebrafish. a**, A diagram showing the lactose and maltose treatment time
716 window and imaging time point. **b-d"**, Confocal imaging analysis of the control, lactose, and
717 maltose treated *Tg(fli1aEP:EGFP-CAAX)*^{ntu666} embryos.

718

719 **Supplementary Figure 8 Pyruvic acid treatment did not cause excessive angiogenesis in**
720 **zebrafish. a**, A diagram showing the pyruvic acid treatment time window and imaging time
721 point. **b**, Confocal imaging analysis of the pyruvic acid-treated *Tg(fli1aEP:EGFP-*
722 *CAAX)*^{ntu666} embryos. **c**, A diagram showing the pyruvic acid treatment time window and
723 imaging time point. **d**, Confocal imaging analysis of the pyruvic acid-treated

724 *Tg(fli1aEP:EGFP-CAAX)*^{ntu666} embryos.

725

726 **Supplementary Figure 9 Overview of the number of genes, total UMIs, and percentage**
727 **of mitochondrial UMIs for the single-cell RNA sequencing. a**, Before filtering. **b**, After
728 filtering. Cell selection criteria: 500< number of genes < 3000; 0< percentage of
729 mitochondrial UMIs < 5%.

730

731 **Supplementary Figure 10 UMAP representation of EC subpopulations. All single cells**
732 **(after filtering) from the control and D-glucose treated were included in this illustration.**

733

734 **Supplementary Figure 11 Confocal imaging analysis of blood vessels in the embryos**
735 **with lenvatinib treatment. a**, A diagram showing the lenvatinib treatment time window and
736 imaging time point. **b**, Confocal imaging analysis of the control and lenvatinib treated
737 *Tg(fli1aEP:EGFP-CAAX)*^{ntu666} embryos. **c**, A diagram showing the lenvatinib treatment time
738 window and imaging time point. **d**, Confocal imaging analysis of the control and lenvatinib
739 treated *Tg(fli1aEP:EGFP-CAAX)*^{ntu666} embryos.

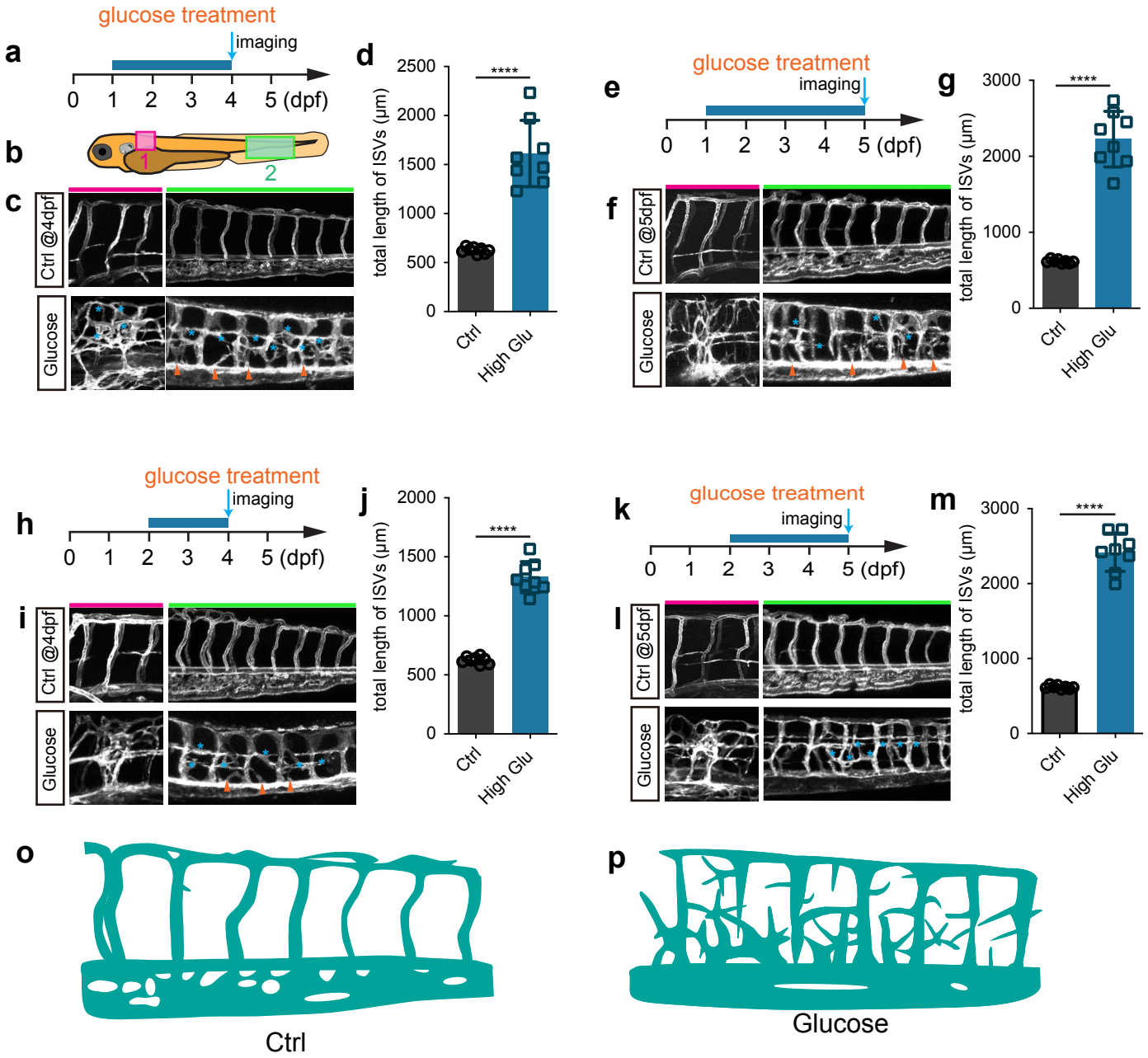
a
glucose treatment
imaging
0 1 2 3 4 5 (dpf)
b
1
2
c
Ctrl @4dpf
Glucose
d
total length of ISVs (μm)
2500
2000
1500
1000
500
0
****
Ctrl
High Glu
e
glucose treatment
imaging
0 1 2 3 4 5 (dpf)
f
Ctrl @5dpf
Glucose
g
total length of ISVs (μm)
3000
2000
1000
0
****
Ctrl
High Glu
h
glucose treatment
imaging
0 1 2 3 4 5 (dpf)
i
Ctrl @4dpf
Glucose
j
total length of ISVs (μm)
2000
1500
1000
500
0
****
Ctrl
High Glu
k
glucose treatment
imaging
0 1 2 3 4 5 (dpf)
l
Ctrl @5dpf
Glucose
m
total length of ISVs (μm)
3000
2000
1000
0
****
Ctrl
High Glu
o
Ctrl
p
Glucose

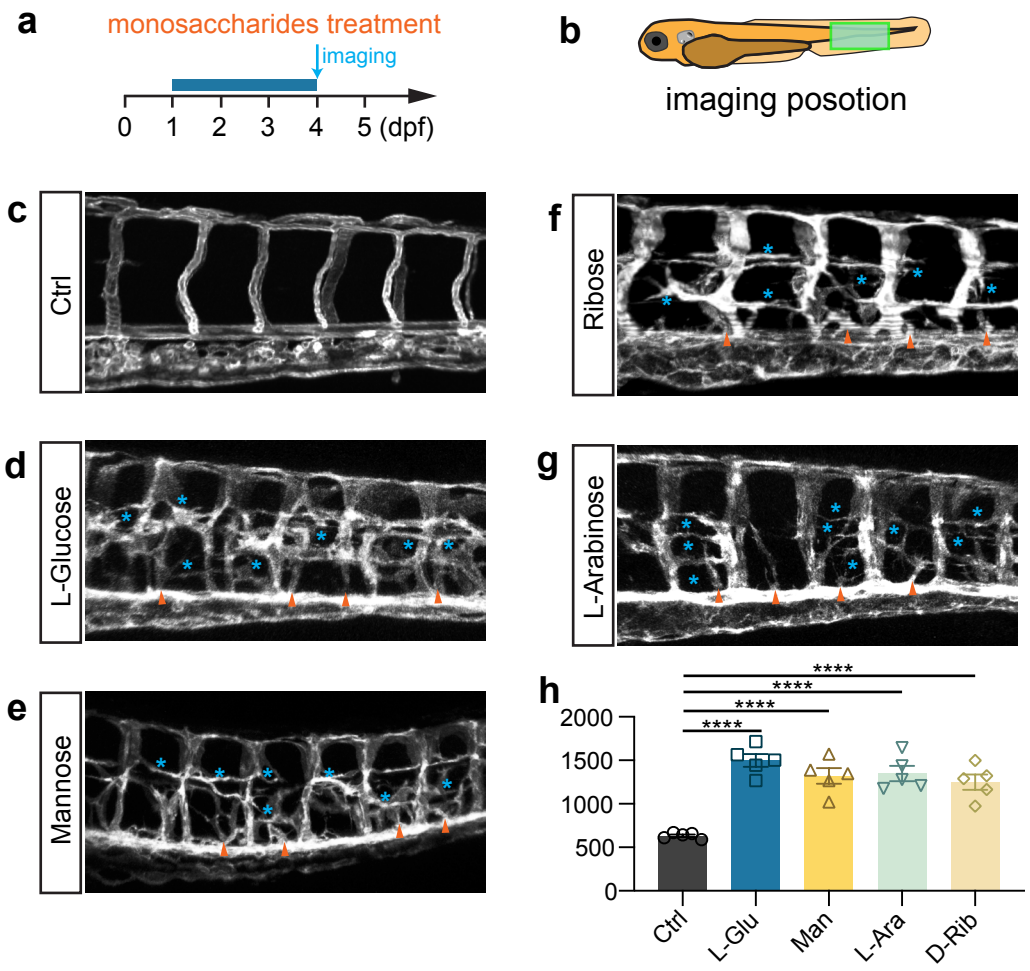
a
monosaccharides treatment
imaging
0 1 2 3 4 5 (dpf)
b
imaging posotion
c
Ctrl
d
L-Glucose
e
Mannose
f
Ribose
g
L-Arabinose
h
2000
1500
1000
500
0
****
Ctrl
L-Glu
Man
L-Ara
D-Rib

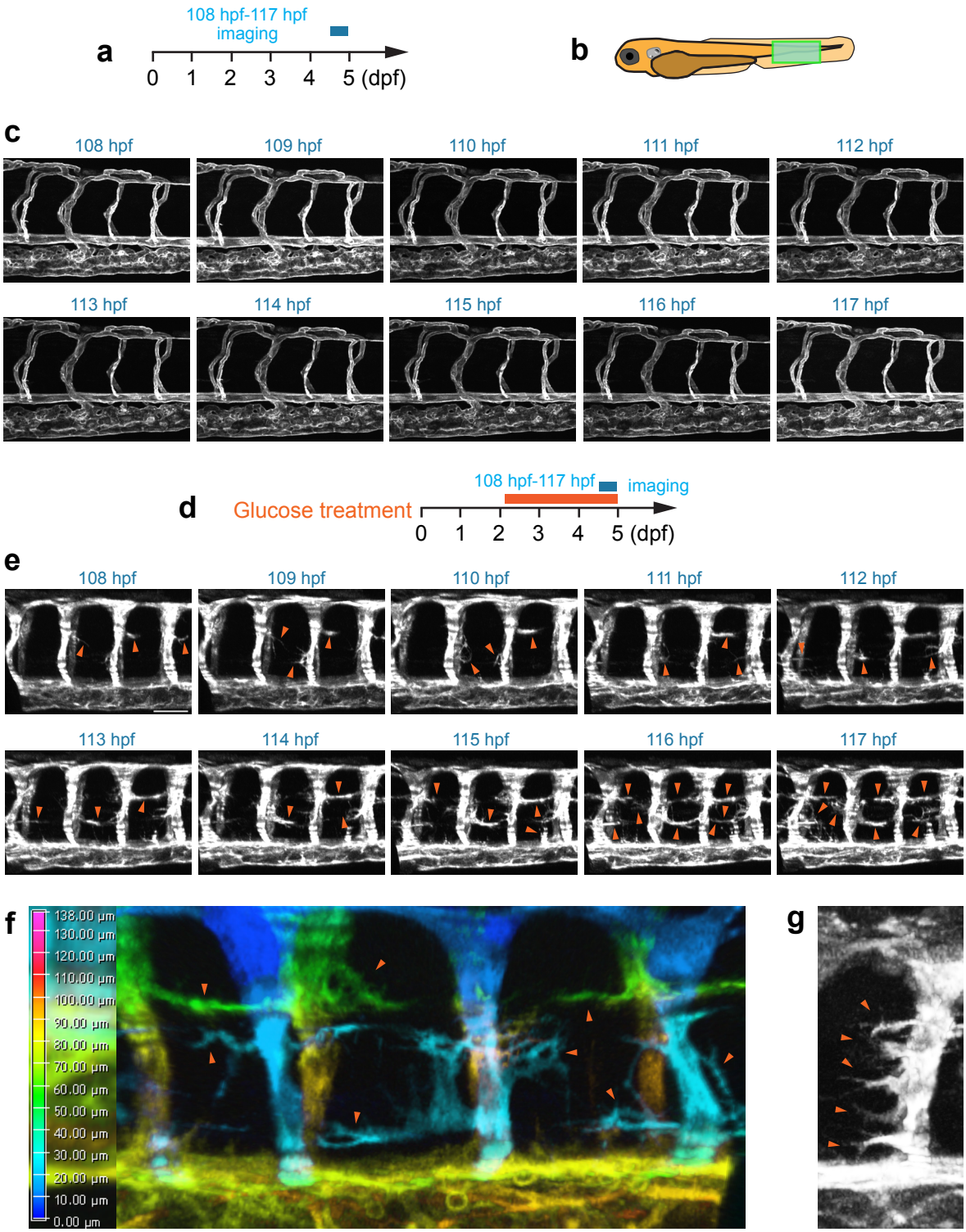
a
108 hpf-117 hpf
imaging
0 1 2 3 4 5 (dpf)
b
c
108 hpf
109 hpf
110 hpf
111 hpf
112 hpf
113 hpf
114 hpf
115 hpf
116 hpf
117 hpf
d
Glucose treatment
108 hpf-117 hpf
imaging
0 1 2 3 4 5 (dpf)
e
108 hpf
109 hpf
110 hpf
111 hpf
112 hpf
113 hpf
114 hpf
115 hpf
116 hpf
117 hpf
f
138.00 µm
130.00 µm
120.00 µm
110.00 µm
100.00 µm
90.00 µm
80.00 µm
70.00 µm
60.00 µm
50.00 µm
40.00 µm
30.00 µm
20.00 µm
10.00 µm
0.00 µm
g

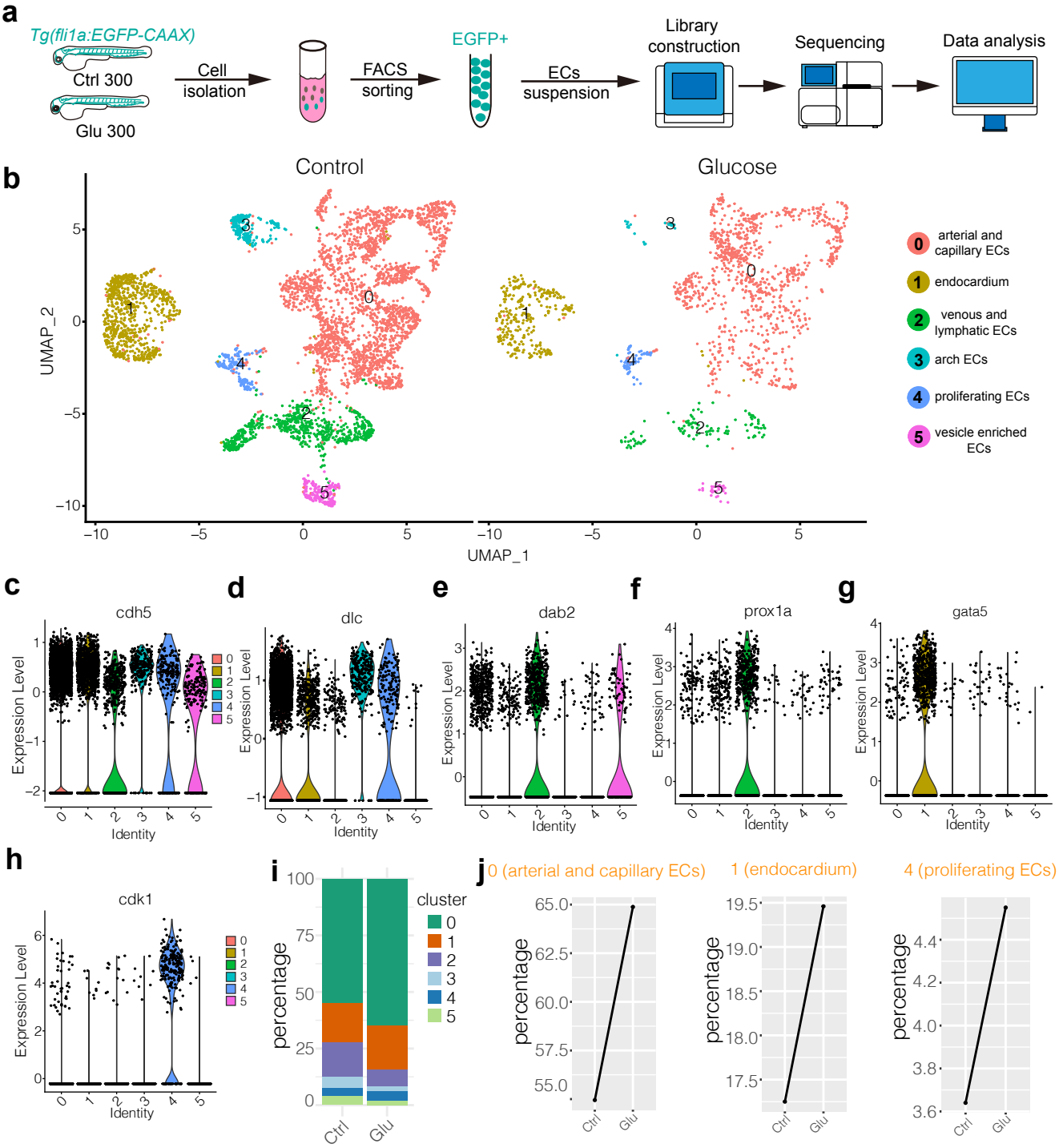
a
Tg(fli1a:EGFP-CAAX)
Ctrl 300
Glu 300
Cell isolation
FACS sorting
EGFP+
ECs suspension
Library construction
Sequencing
Data analysis
b
Control
Glucose
UMAP_2
UMAP_1
0 arterial and capillary ECs
1 endocardium
2 venous and lymphatic ECs
3 arch ECs
4 proliferating ECs
5 vesicle enriched ECs
c
cdh5
d
dlc
e
dab2
f
prox1a
g
gata5
Expression Level
Identity
h
cdk1
i
percentage
cluster
Ctrl
Glu
j
0 (arterial and capillary ECs)
1 (endocardium)
4 (proliferating ECs)
percentage

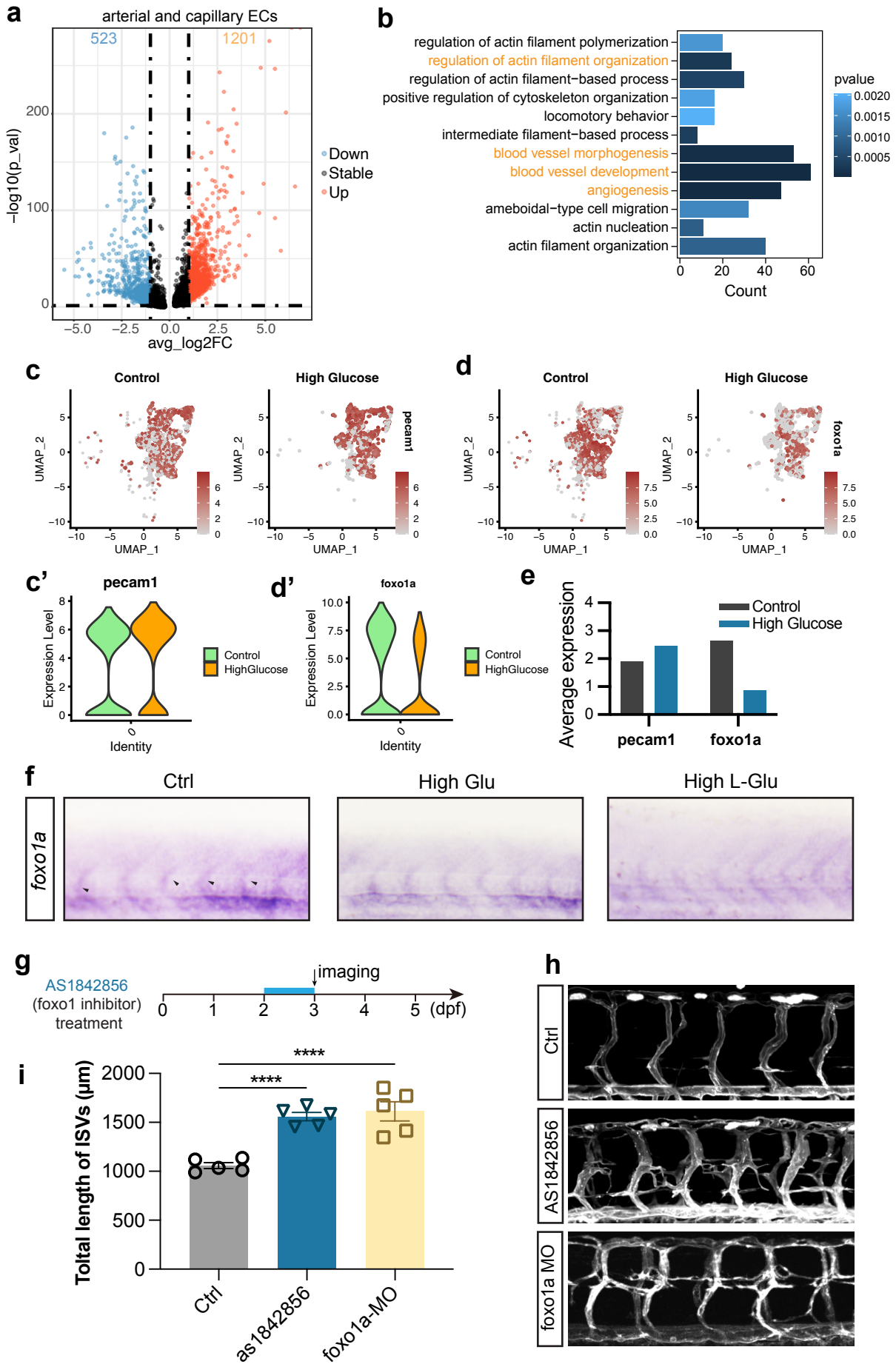
a
arterial and capillary ECs
523
1201
−log10(p_val)
avg_log2FC
Down
Stable
Up
b
regulation of actin filament polymerization
regulation of actin filament organization
regulation of actin filament−based process
positive regulation of cytoskeleton organization
locomotory behavior
intermediate filament−based process
blood vessel morphogenesis
blood vessel development
angiogenesis
ameboidal−type cell migration
actin nucleation
actin filament organization
Count
pvalue
c
Control
High Glucose
pecam1
UMAP_1
UMAP_2
d
foxo1a
c'
Expression Level
Identity
HighGlucose
d'
e
Average expression
pecam1
foxo1a
f
Ctrl
High Glu
High L-Glu
foxo1a
g
AS1842856
(foxo1 inhibitor)
treatment
imaging
(dpf)
h
Ctrl
AS1842856
foxo1a MO
i
Toltal length of ISVs (μm)
****
Ctrl
as1842856
foxo1a-MO

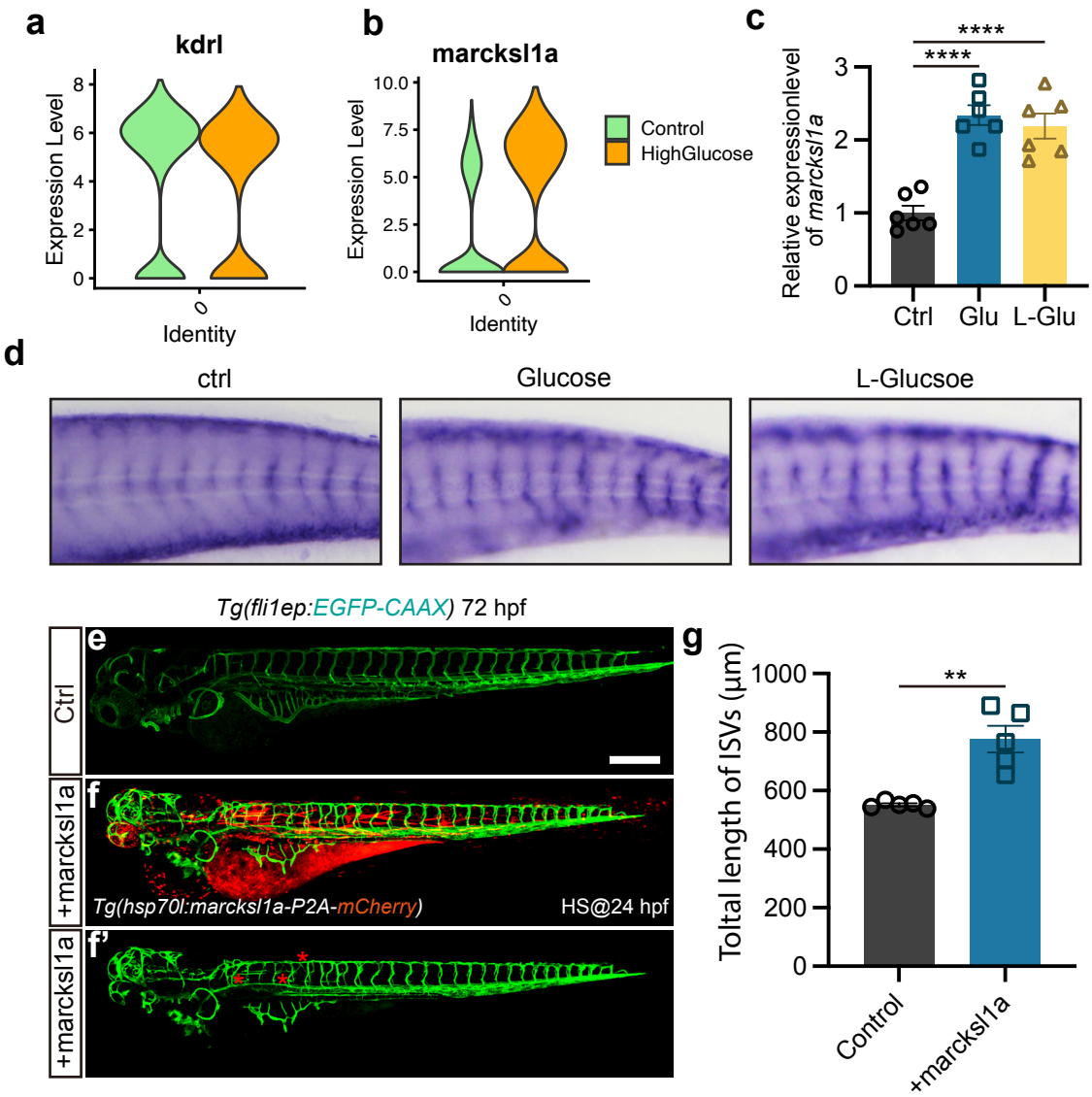
a
kdrl
Expression Level
Identity
b
marcksl1a
Expression Level
Identity
Control
HighGlucose
c
Relative expressionlevel of marcksl1a
****
****
Ctrl
Glu
L-Glu
d
ctrl
Glucose
L-Glucsoe
Tg(fli1ep:EGFP-CAAX) 72 hpf
Ctrl
+marcksl1a
+marcksl1a
e
f
f'
Tg(hsp70l:marcksl1a-P2A-mCherry)
HS@24 hpf
g
Toltal length of ISVs (μm)
**
Control
+marcksl1a

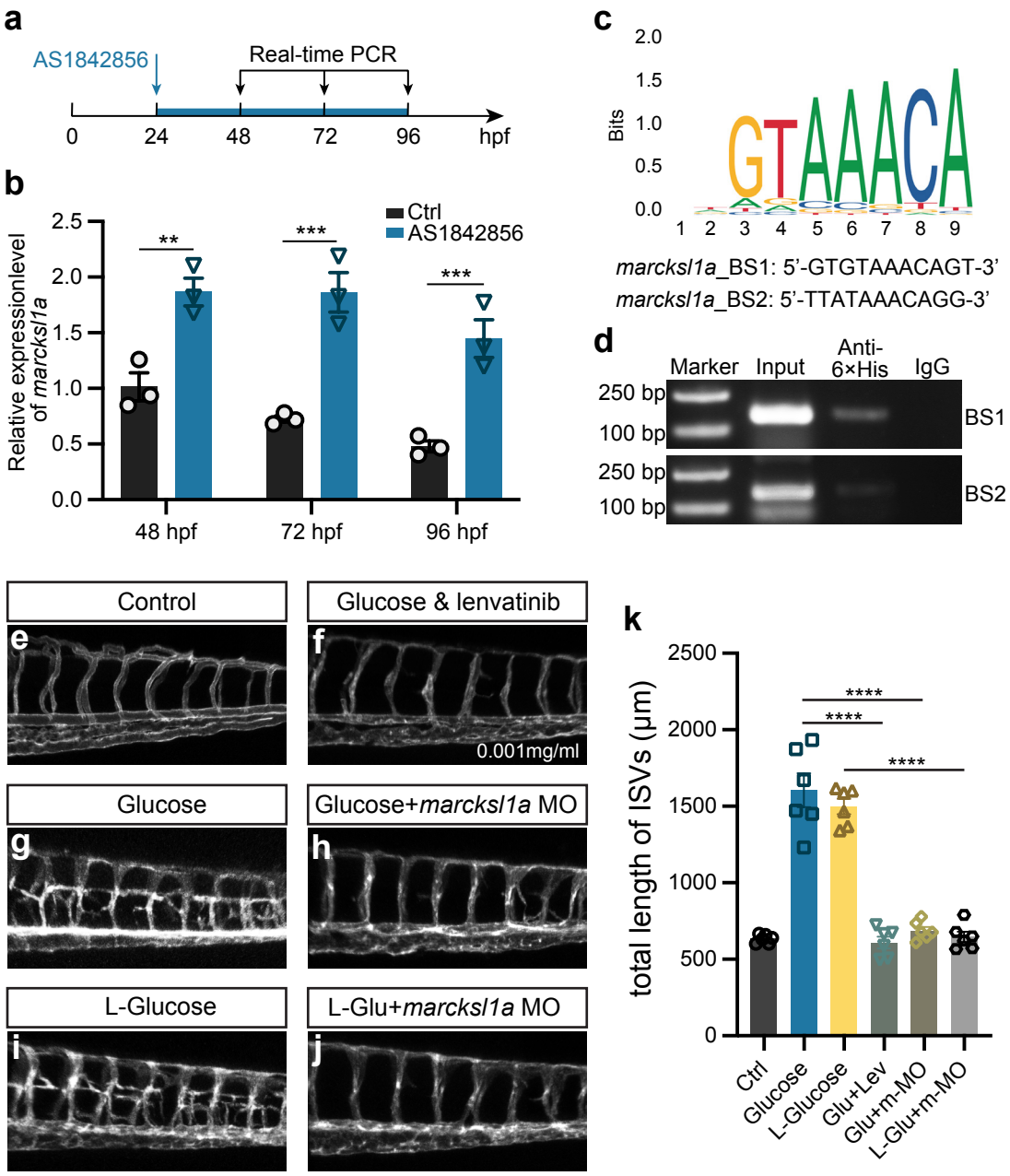
a
AS1842856
Real-time PCR
0
24
48
72
96
hpf
b
Ctrl
AS1842856
Relative expressionlevel of marcksl1a
2.5
2.0
1.5
1.0
0.5
0.0
**
***
***
48 hpf
72 hpf
96 hpf
c
Bits
2.0
1.5
1.0
0.5
0.0
1 2 3 4 5 6 7 8 9
marcksl1a_BS1: 5'-GTGTAAACAGT-3'
marcksl1a_BS2: 5'-TTATAAACAGG-3'
d
Marker
Input
Anti-6×His
IgG
250 bp
100 bp
BS1
250 bp
100 bp
BS2
Control
Glucose & lenvatinib
0.001mg/ml
Glucose
Glucose+marcksl1a MO
L-Glucose
L-Glu+marcksl1a MO
k
total length of ISVs (μm)
2500
2000
1500
1000
500
0
****
****
****
Ctrl
Glucose
L-Glucose
Glu+Lev
Glu+m-MO
L-Glu+m-MO